DIII-D Research to Address Key Challenges for ITER and Fusion Energy

R.J. Buttery[1] and the DIII-D Team

[1]General Atomics, PO Box 85608, San Diego, California 92186-5608, USA
E-mail contact of main author: buttery@fusion.gat.com

Abstract. The DIII-D tokamak has addressed critical challenges in preparation for ITER and the next generation of fusion devices. The robustness and performance of ITER scenarios was expanded with edge localized mode suppression demonstrated with a reduced coil set, disruption heat load and runaway electron mitigation, extending the ITER baseline scenario to low torque, and developing the promising QH mode to high Greenwald fraction. Work with the ITER Test Blanket Module simulator has developed error correction that reduces heat loads by 80% and recovers most of the performance degradation. The path to fusion energy has been advanced using DIII-D's flexible heating systems to develop a high β_P steady state scenario at low neutral beam torque, a 1 MA fully noninductive hybrid scenario, and sustain a high l_i regime to β_N=5. The compatibility of high performance regimes with edge solutions has been demonstrated including: ELM suppression in fully non-inductive plasmas and sustained high performance in radiative divertor conditions and new divertor geometries such as the snowflake. A strong science program identifies underlying physics mechanisms to guide new developments and provide robust projection to future devices. Transport studies show the approach to burning plasma conditions increases long wavelength turbulence and thus thermal and particle transport. Pedestal models predicted the path to a new super H-mode scenario, achieved with doubled pedestal pressure, while kinetic models identify separate energy and particle transport mechanisms near the separatrix. Lithium pellets lead to a bifurcation to a wider, higher pedestal. The origin of intrinsic rotation is explained by a kinetic loss-cone model, while the bifurcation to H-mode is found triggered by turbulence driven rotational shear and build up of ion diamagnetic flows. Detachment studies measuring behavior to <1 eV with 2D Thomson scattering identify a radiation shortfall in simulation models. Upgraded 3D magnetics validate linear MHD predictions of plasma response. Energetic particle studies validate fully nonlinear toroidicity-induced Alfvén eigenmode simulations, but also point to a new paradigm critical gradient model to project behavior. Future plans target key needs to anticipate burning plasma physics with torque free electron heating, the path to steady state with increased off axis currents, and a new divertor solution for future reactors.

1. Introduction

The central theme of the DIII-D research program is to improve scientific understanding in order to develop and project better solutions for fusion energy. Research targets both preparation for ITER, and the longer range path to fusion energy. These goals are advanced by equipping the facility with high levels of operational flexibility, to access and explore relevant regimes, and diagnostics to identify physics mechanisms. Studies are underpinned by close collaboration with theory and simulation initiatives to interpret and guide development

Results capitalize on several enhancements of the facility. New disruption mitigators and diagnostics enabled physics tests of ITER candidate techniques. Real-time electron cyclotron deposition control provided routine stability and profile control. A major 3D magnetics upgrade has identified key facets of plasma 3D-field response. A periscope, with infrared visible imaging, together with coherence flow imaging and high-resolution sub-eV divertor Thomson scattering, revealed new insights in edge physics. Main ion charge exchange recombination (CER) provided crucial constraints to transport and rotation models. A lithium dropper led to improved pedestals.

This paper is organised on a topical basis, starting with the most urgent issues for ITER. Section 2 concentrates on the achievement and physics behind edge localized mode (ELM) control and improved pedestal. Section 3 addresses disruption mitigation. In Sec. 4 we explore how core behavior changes under increasingly burning plasma-like conditions, while Sec. 5 deals with the development of robust scenarios for ITER and underlying stability issues. We then turn toward issues of fusion energy, with development of high performance steady state core plasmas in Sec. 6, and the physics basis for improved boundary solutions in

Sec. 7. Section 8 concludes with an overview of achievements and discussion of the future direction for the DIII-D program.

2. Achieving a Robustly ELM-Stable and High Performance Pedestal

The tokamak pedestal is the critical area governing plasma performance, establishing the basis for core fusion performance, but giving rise to ELMs, which must be mitigated to avoid first wall erosion. DIII-D has expanded access to ELM suppressed regimes, developed new higher performance pedestals and answered critical physics questions.

By exploiting DIII-D's flexible 3D field coil arrays and upgraded magnetics, it has been possible to identify for the first time penetration of the RMP at the pedestal top as the likely physics mechanism behind resonant magnetic perturbation (RMP) ELM suppression – [1,2]. This was achieved by extending the technique to n=2 RMPs, which allowed the field structure to be continuously varied by rotating the field from an upper coil array relative to a lower array. This leads to periods of ELM suppression and ELMing activity (Fig. 1). Crucially, the transition to suppression is accompanied by a non-linear increase in magnetic response in new high field side magnetic measurements, consistent with a field line pitch resonant field [3]. This is accompanied by a decrease in temperature and pressure gradients near the pedestal top, limiting pedestal height below the kink-ballooning stability limit. Here, perpendicular electron rotation is brought to zero, consistent with stationary island formation (also seen with n=3 RMP ELM suppression). This is characteristic of a transition from shielding to tearing at the pedestal top, and is replicated by two fluid MHD calculations with the M3D-C1 code, which predict stochastized islands at the pedestal top. This stochastization is expected to further increase cross-field transport in the region [4] and leads to a predominantly n=0 profile response, explaining the lack of observed helical island structure with suppression. Encouragingly, these simulations predict the same effect in ITER.

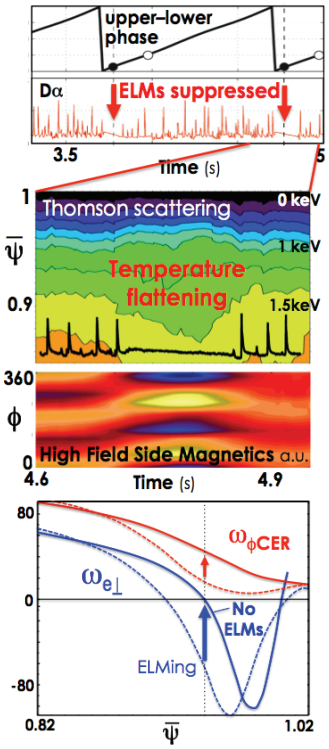

Fig. 1: n=2 upper-lower RMP phase rotation leading to periods of ELM suppression, temperature flattening, magnetic and rotation responses.

Further confidence is gained from the successful application of n=3 RMP ELM suppression as successive coils are turned off (Fig. 2) [5], while maintaining suppression at similar coil current and confinement levels. M3D-C1 simulation indicates that the reduction in the primary n=3 harmonic is compensated by additional n=2, 4 and 5 sidebands. RMP ELM control has also been extended to low torque helium plasmas with dominant electron heating, providing important validation for the ITER research plan which seeks to establish the basis for ELM suppression in its non-nuclear phase, and to fully non-inductive steady state regimes, where it results in a factor 5 reduction in ELM size, offering promise for future steady state devices. Generally, behavior is consistent with the EPED model [6] of a peeling ballooning limit governing ELM onset, with data and model showing pedestal pressure increasing with density and good confinement in cases that are close to RMP threshold for ELM suppression. Encouragingly, impurities are not observed to accumulate in RMP ELM suppressed plasmas.

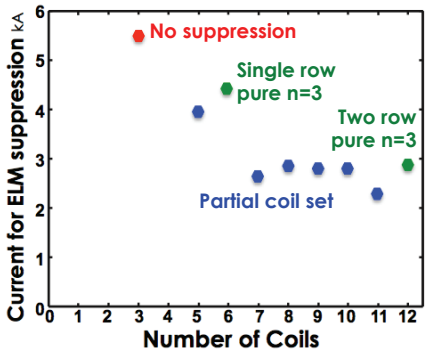

Fig. 2: Current required for ELM suppression as coils turned off.

Breakthroughs have also been made in developing the QH mode regime for ELM stable high performance operation [7]. This regime is sustained by a benign edge harmonic oscillation (EHO) which replaces the ELM, sitting close to the peeling-ballooning limit. By increasing plasma shaping and fuelling, it has been possible to extend QH mode to high Greenwald density fraction (Fig. 3), establishing compatibility of the EHO with high density regimes. This validates the EPED description of QH mode access, which further project that ITER will be able to access this regime. Nonlinear JOREK modeling of DIII-D QH-mode plasmas, [8] indicates saturation of peeling-ballooning modes, hypothesized to account for the EHO, with the saturation considered likely to be due to formation of islands and an ergodic layer in the pedestal. In addition to regulating edge electron transport, the EHO, based on CER measurements of fluorine confinement, is found to give adequate levels of impurity flushing, comparable to 40 Hz ELMs in DIII-D, which both give good impurity control. Figure 4 shows this to be considerably better than low frequency (10-15 Hz) ELMs that have similar character to unmitigated ELMs in the ITER baseline which lead to impurity accumulation. These benefits are also borne out in better confinement variants of QH mode with increased ExB shearing rates at low torque. Thus QH mode shows great promise for ITER, with performance on DIII-D demonstrated at the ITER baseline β_N, H_{98} and q_{95} for 20 confinement times, though work remains to achieve this level of performance at ITER-relevant torque.

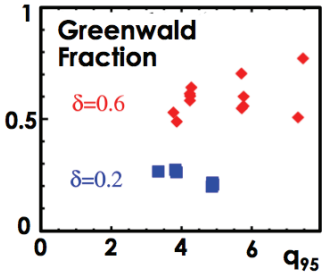

Fig. 3: Extension of QH mode to high Greenwald density.

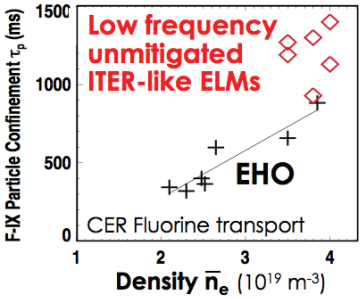

Fig. 4: EHO impurity flushing compared to low frequency ITER-like unmitigated ELMs.

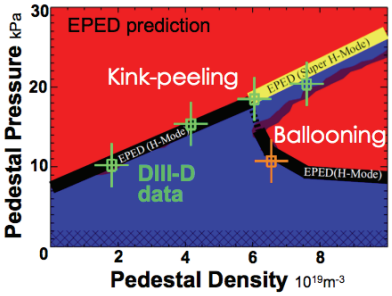

Fig. 5: Access to super-H mode at high shaping.

Further optimization of the pedestal has led to a new regime of high performance, dubbed "super-H mode' [9] which doubles pedestal height over the usual peeling ballooning limits. To achieve this, EPED predicts increased shaping to open a valley of improved pedestal stability between peeling-kink and ballooning branches of stability. This has been navigated (Fig. 5) using the benign EHO in QH mode regimes to skirt the valley edges as density is raised leading to H_{98pby2}~1.4 and β_N up to 3.1. Pedestal heights are double those on the ballooning branch (that correspond to standard H-mode), suggesting this an exciting approach for transforming prospects for fusion energy. In a separate development, injection of lithium pellets also led to dramatic improvements in pedestal performance, in this case by causing edge turbulence to rise leading to a broader, less steep but much higher pedestal [10].

In this work, EPED provides an important tool in predicting pedestal height. While it has been validated on multiple devices, new experiments on DIII-D provide the first direct evidence for the mechanisms involved. The model assumes kinetic ballooning mode (KBM) places a limit on pressure gradient, while pedestal width grows until a peeling-ballooning mode is encountered (triggering the ELM). Measurements of inter-ELM activity show quasi-coherent density

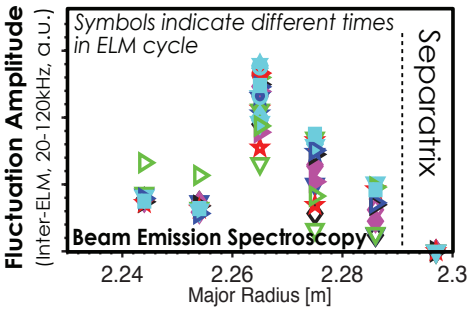

Fig. 6: KBM-consistent density fluctuations at the pedestal top.

(Fig. 6) [11] fluctuations at the pedestal top correlating with limitations in temperature gradient consistent with predicted KBM behavior and thresholds. This gives further confidence in EPED as an effective tool for projecting to ITER.

Understanding the details of profiles, rotation generation, impurity transport and fuelling requires a deeper treatment. Here main ion CER and high resolution reciprocating probe measurements in electron cyclotron heating (ECH) H-mode (Fig. 7) are consistent with a kinetic loss cone model of rotation generation, whereby asymmetric thermal ion losses from the distorted Maxwellian inside the plasma lead to an intrinsic rotation. New edge main ion CER measurements play a crucial role in determining the bulk rotation, as these measurements show dramatically different inferred rotations from carbon. Transport studies show this edge rotation correlates with rotation in the core, though effects of MHD and turbulence deeper in can give rise to profile variations. A fuller description of the pedestal with XGC0 kinetic simulation provides greater insight [12], showing energy and particle transport to be decoupled, with ion energy transport set primarily by collisionless orbit loss of deuterium ions in the thermal tail (validating the above concepts) while particle behavior is governed by anomalous transport of colder bulk ions. It is expected that the kinetic effects that lead to intrinsic velocity near the separatrix in low collisionality plasmas on DIII-D will generate a similar edge flow in ITER.

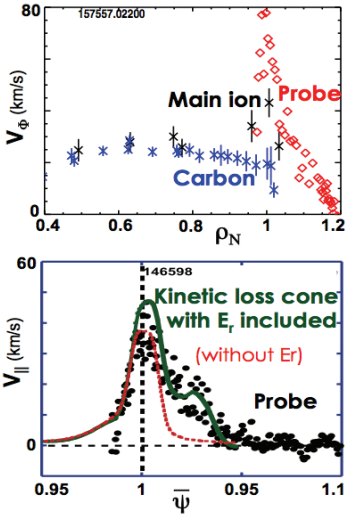

Fig. 7: Measurements confirm kinetic intrinsic model rotation.

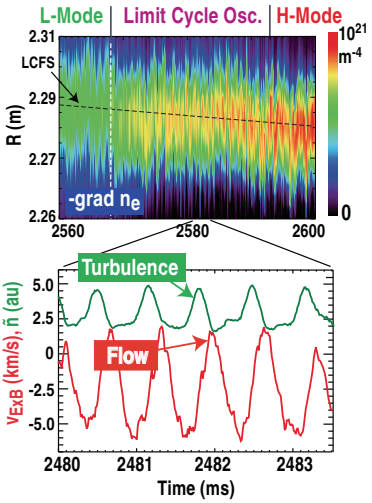

Fig. 8: L-H limit cycle behavior and longer time-scale gradient rise.

Finally, turbulence diagnostics are providing critical understanding on the formation of the pedestal – the L-H transition. 2D beam emission spectroscopy (BES) measurements show how turbulence in an L-mode edge increases leading to Reynolds stress. This drives a sheared flow, which shears the turbulence apart leading to the H-mode bifurcation [13]. In some plasmas this leads to a cyclic behavior (Fig. 8), where the H-mode only becomes sustained over longer timescales. Here Doppler backscattering (DBS) and CER capture the same turbulence-flow-generation effect, but high flow shear state is not sustained, and the plasma back-transitions. It is only after strong pedestal pressure gradients are established that the H mode becomes sustained, indicating the key role of pressure driven ion diamagnetic flow in locking in the H-mode transition through a rise in ExB shear [14]. However, other theories suggest these transitions may be explainable purely through mean field momentum transport equation [15].

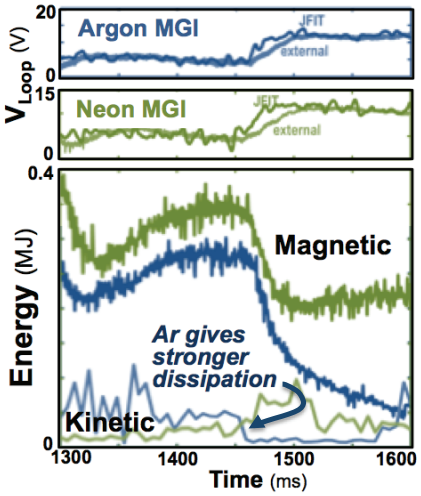

Fig. 9: Argon MGI (blue) leads to greater dissipation of RE kinetic energy, than neon MGI (green) despite larger induced loop voltage.

3. Disruption Mitigation

DIII-D research is establishing the principles and techniques for ITER's disruption mitigation system. The most critical issue is the management of runaway electron

(RE) beams, predicted to be strongly driven in ITER, requiring a control solution to prevent wall damage. DIII-D has unique capabilities to generate, diagnose, control and dissipate REs, including ITER-like actuators and a "slide-away" low-density regime to cleanly characterize RE onset [16]. Encouragingly, these show high levels of anomalous RE dissipation in both slide-away cases and RE plateaus following a disruption. Reconstructions of the energy distribution function have been performed by combining hard x-ray (HXR), mid x-ray(MXR), soft x-ray (SXR), and synchrotron emission data, to provide for the first time an estimate of the RE beam kinetic energy and dissipation mechanisms. This has been used to establish that high-Z (argon) massive gas injection (MGI) gives significantly stronger dissipation than mid-Z (neon) MGI (Fig. 9). Experiments confirm that the RE velocity pitch angle dominates the synchrotron emission pattern, leading to crescent-shaped synchrotron emission patterns in the visible and IR, with emission considerably increased by high Z emission. Further, in a first of a kind demonstration, a new ITER-prototype "bent-tube" neon shattered pellet injector (SPI) system was found able to suppress runaways during the current quench phase, when they are usually driven to large amplitudes, showing great promise for ITER [17].

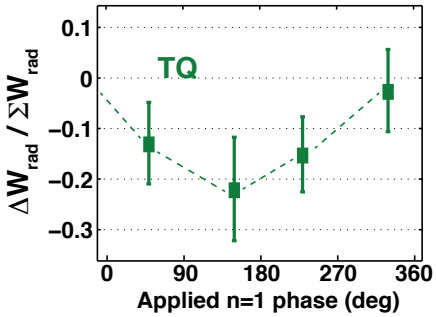

Fig. 10: Measured radiated energy asymmetry vs applied n=1 error field phase during TQ.

Thermal quench (TQ) mitigation also shows encouraging trends [18], with MGI found not to lead to excessively localized heat loads from radiation asymmetry, and behavior validating NIMROD simulations [19]. Studies with n=1 error fields have confirmed the predicted importance of an n=1 mode in determining the phase of toroidal radiation peaking (Fig. 10). These asymmetries are relatively modest compared to ITER assumptions. The initial mode phase is found to be 180 degrees away from injector location. It then rotates with the plasma and any applied error field. Other studies showed <30% asymmetry in radiation during the thermal quench, irrespective of relative timing or mix of two toroidally and poloidally separated gas injectors. Wall heat loads were found distributed away from injector location in IR imaging. Direct matched comparisons of MGI to the new ITER prototype neon SPI reveal the SPI leads to more rapid quenching with deeper penetration and particle assimilation, than an equivalent quantity of MGI. Finally, in the case of vertical displacement, mitigation of heat loads, forces and halo currents was effective, and depended only modestly on injector location relative to displacement path, though earlier mitigation gave clear advantages in reducing heat loads from vertical displacement events (VDEs).

4. Preparing for Burning Plasma Conditions

Energy, particle and momentum transport will differ in burning plasmas compared with most present devices. Instead of high torque ion heating with core fuelling, burning plasmas will be heated through the electrons, without core fuelling or significant torque injection. This may lead to substantial changes in transport and stability, which must be understood if we are to re-optimize regimes for burning plasma conditions. DIII-D is confronting this challenge with neutral beam injection (NBI) torque control and ECH to access the relevant regimes, probe the physics and develop integrated scenario solutions, so that high performance burning plasmas can be readily achieved in ITER with confident projection capabilities.

Turbulent Transport

A significant reduction in confinement is found in low torque ITER baseline-like plasmas when electron heating is applied, with H_{98} falling from 1.02 to 0.88 when 3.3 MW of ECH is applied to a plasma with 3 MW neutral beam heating. Increasing T_e/T_i via ECH leads to

increased particle loss and lower rotation, associated with large rises in low and intermediate *k* turbulence, with resulting profiles well matched by trapped gyro-Landau fluid (TGLF) calculation. To explore this physics, transport studies have focussed on how turbulence, transport and confinement change approaching burning plasma conditions: low applied torque and higher electron heating.

Experiments that systematically varied torque demonstrated for the first time the radial and wavenumber dependencies of the ExB shear paradigm of turbulence suppression [20]. These reveal a sharp rise in low k turbulence ($0.1<k_{\perp}\rho_s<0.5$), observed in density fluctuations from BES (Fig. 11), correlated with a fall in energy confinement at lower torque and toroidal rotation, while particle confinement exhibits a more modest change. This behavior is matched by GYRO predictions of increased linear growth rates, consistent with observed reductions in ExB shear rates. This indicates that it is important to explore the transport optimization for burning plasmas in low rotation conditions. It also highlights important directions for scenario development such as rotation shear generation through neoclassical toroidal viscosity as used in the QH-mode scenario, and development of improved pedestals.

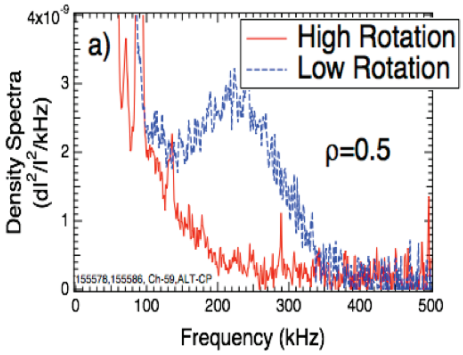

Fig. 11: Increase in low k turbulence at low rotation.

The effects of increasing T_e/T_i have been explored in low rotation QH-mode plasmas, which provide a quiescent background to observe behavior. Here, increased electron heating via ECH is found [21] to significantly increase TEM scale fluctuations observed with DBS measurements (Fig. 12), which also identify core coherent fluctuations as candidate-TEM modes. GYRO simulations suggest this is due to a strong sensitivity of TEM growth rates on T_e/T_i. Non-linear simulations also capture the frequency spectrum and match particle and thermal fluxes. These effects increase both energy and particle transport, leading to decreased density peaking. This suggests a possible self-limiting mechanism in burning plasmas, where increasing α power will drive more TEMs, thereby reducing density peaking.

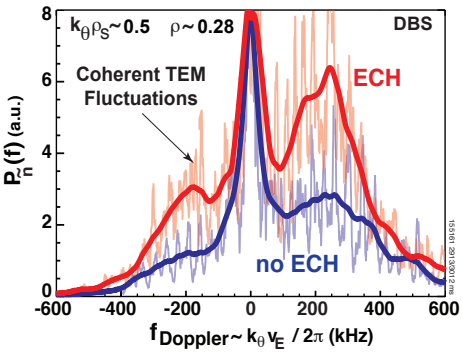

Fig. 12: Increase in TEM turbulence with electron heating in QH mode.

These basic trends have also been observed in plasmas with dominant electron heating at lower β, where a transition from ion temperature gradient (ITG) to TEM behavior is observed when NBI heating is replaced with ECH [22]. This leads to increased outward particle diffusion, as predicted by TGLF, although at larger radii ($\rho>0.5$) this is partly countered by increased inward pinch. Observations help explain ASDEX Upgrade results [23], which found an increase in density peaking with decreasing collisionality *and* rotation. DIII-D studies varied these separately to find that increased ExB shearing rates, rather than collisionality or inward roto-diffusion, suppress turbulence to alter profiles. Work has also continued to explore basic turbulent physics in dominant electron-heated regimes, confirming gyrokinetic and gyrofluid model (GYRO and TGLF) of stiffness in electron transport as TEMs become excited [24]. However, ion heat flux remains under-predicted. These studies represent powerful tests of turbulence models, providing validation at 3 levels – profiles, transport and turbulence amplitudes – critical to projecting techniques to reach required performance in burning plasmas.

Fast Ion Behavior

Fusion energy also requires good confinement of energetic fast ions for efficient heating and current drive. However, fast ions can drive Alfvén eigenmodes (AEs), which in turn redistribute the fast ions, as observed in some steady state plasmas [25]. Experiments on DIII-D have identified a critical gradient behavior behind this effect. It is found that as fast ion pressure gradient rises above a threshold, redistribution effects rise rapidly (figure to appear in forthcoming letter [26]) leading to a limit in fast ion density. This behavior is hypothesized to be due to overlap of many small amplitude AE resonances. This potentially transforms predictive capability, greatly easing projection to future facilities. The work is complemented by comparisons to the first fully nonlinear simulations of AE and fast ion evolution [27], which match mode structure and saturation levels well, confirming the physics on which critical gradient models are founded.

Fast ion redistribution can also lead to localized heating of the tokamak walls, particularly when 3D fields are present. For example, Fig. 13 shows how RMP fields used for ELM suppression can eject a significant fraction of confined fast ions in the plasma edge region [28]. Here brief notches in RMP field lead to rises in fast ion density while divertor heat loads fall substantially. Results are well represented by the SPIRAL full orbit code, which models the interaction of a realistic beam ion distribution with the 3D field, including ideal MHD response from M3D-C1, to predict losses from $\rho>0.7$, mostly to the divertor. Such prompt losses are also observed with internal modes such as NTMs and AEs, potentially enabling diagnosis of internal response. Further losses from multiple modes can combine nonlinearly to lead to greatly enhanced ion loss mechanisms. This highlights the importance of optimizing 3D field geometry to minimize fast ion losses, as accomplished in the TBM error field correction mentioned in the previous section.

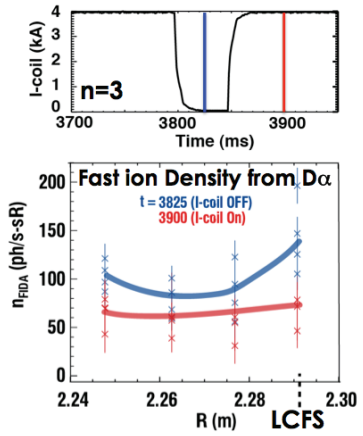

Fig. 13: Fall in fast ion density as RMP turns on.

5. Realizing Stable Integrated Burning Plasma Scenarios

The optimization of operating scenarios for burning plasma conditions raises key challenges for stability and scenario development. Low torque operation makes the plasma more susceptible to MHD driven by 3D "error" fields or inherent instability; this behavior must be understood and better controlled. Techniques for establishing ELM control and radiative divertor conditions must be integrated. Regimes need to be re-optimized for transport and pedestal behavior in burning plasma relevant conditions.

A foundational issue is the response of the plasma to 3D fields – effective models are critical to understanding how to optimize their use for control and avoid deleterious "error field" effects. To explore this a major upgrade to the DIII-D magnetics diagnostic was implemented, particularly with improved high field side arrays to discriminate models. Measurements show that MHD models describe the structure of the response relatively well (Fig. 14,

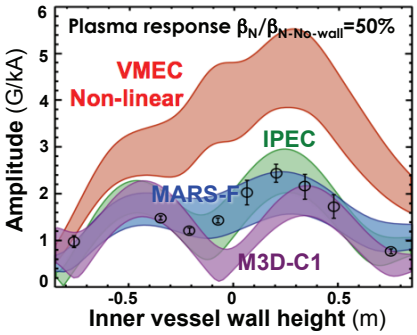

Fig. 14: Comparison of 3D plasma response to MHD models.

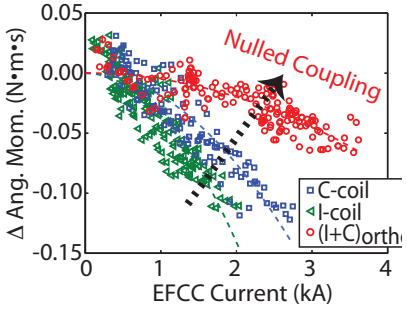

Fig. 15: Fields with nulled coupling (red) to least stable ideal mode have a weak effect on plasma rotation.

MARS-F, IPEC). However, two fluid M3D-C1 simulations reveal sensitivities to assumptions on edge conductivity and single/two fluid MHD, while a non-perturbative MHD simulation (VMEC) tends to over-predict response.

Thus ideal MHD plays a major role in 3D field response, and further experiments show that this is primarily governed by a single "least stable" ideal mode for n=1 fields. This is confirmed by experiments measuring neoclassical toroidal viscosity (NTV) braking of plasma rotation [29]. Here, while fields from internal and external coil arrays separately lead to braking, combining them to null out coupling to the least stable ideal mode nearly eliminates braking (Fig. 15) and avoids driving locked mode (not shown), even at very high field amplitude. The consistency between these two very different approaches, one based on localized flux surface field penetration and the other on global braking, is further evidence of a single mode response. This positive result indicates 3D error field effects may be readily compensated through correction that minimizes just one component of the field. The work has also established a non-disruptive means of optimizing error correction through plasma rotation as a now-routine tool in DIII-D.

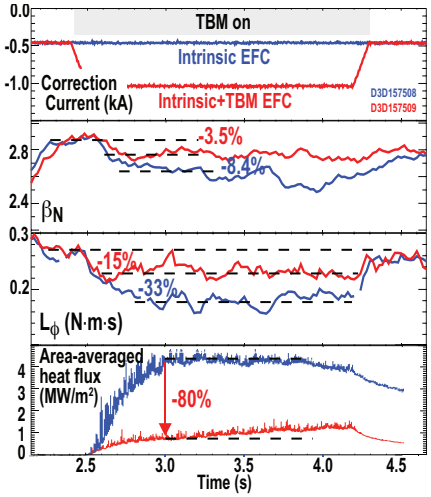

Fig. 16: TBM degradation mitigated with additional correction fields.

Single-component error field compensation has been applied to the key challenge of the Test Blanket Module (TBM) in ITER. A TBM simulator in DIII-D is found [30] to cause confinement degradation and localized heat loads from plasma braking and fast ion loss – a particular issue for higher β alternatives to the ITER baseline such as used here (Fig. 16). However, by using an optimal n=1 correction field, more than half the degradation is avoided, together with an 80% reduction in the localized heat flux to nearby tiles. At low torque the TBM is found to have more serious effects, braking the plasma leading to rotation collapse and locked mode disruption. However, careful tailoring of n=1 correction fields is found to avoid these effects, even at virtually zero torque and maximum amplitude (ITER-relevant level) of TBM field in a high collisionality version of the ITER baseline plasmas. In contrast, variations in addition-al n=2 correction fields are found to have a weak effect.

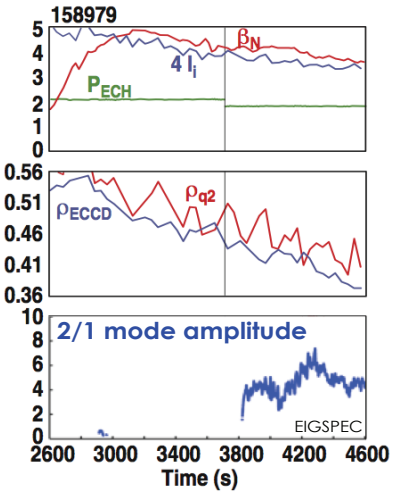

Fig. 17: Real time NTM suppression at high β_N.

The other critical stability issue for ITER is tearing modes. Previous work developing real time tearing control with localized ECH current drive, has been extended with real time ECH deposition calculation, Thomson scattering fitting and faster mirrors, enabling the technique to be applied in evolving high β_N scenarios such as the "high l_i" regime (Fig. 17). Control is lost when ECH power falls.

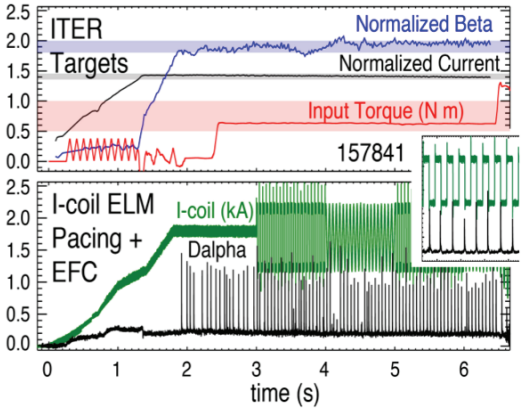

Fig. 18: ITER baseline demonstration at low torque without need for ECCD NTM control.

These issues become crucial in developing the ITER baseline at low torque, where the rotation profile can anomalously hollow and collapse leading to disruption. This requires good error field correction and tearing mode avoidance strategies. Encouragingly, work has found that stability to low n tearing modes, which tend to be destabilized at high torque, and slow and lock as torque is ramped down, is improved when a low torque start up is applied instead. However, large ELMs and an associated impurity build up can still trigger 3/2 modes and rotation collapse. Here, ELM pacing with I-coil modulation proved effective in triggering more rapid ELMs that avoided impurity accumulation and the tearing mode. This enabled demonstration of a Q_{eq}=10 ITER baseline at low torque without the need for ECCD mode control (Fig. 18) [31]. In a final development, a technique for burn control has been developed for ITER [32] using 3D fields to regulate pedestal height and confinement to deliver nearly constant stored energy despite significant power excursions (Fig. 19). This provides a powerful basis to fast regulation of fusion power ($P_{Fus} \sim H_{98}^{5.3}$).

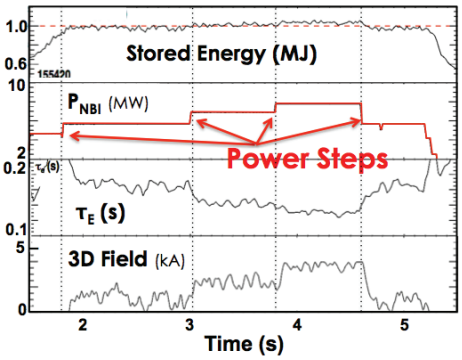

Fig. 19: Real time 3D pedestal regulation will provide effective burn control.

A key challenge emerging from this work is to develop discharges at ITER-relevant torque with ELM control. Thus studies are now exploring how to favorably combine elements of ELM amelioration with effects that improve transport and stability, such as profile modification (hybrid regimes) or neoclassical toroidal viscosity, to achieve Q_{eq}=10 more robustly, and if possible with reduced current to lower disruption risks.

6. The Path to Steady State Fusion

To achieve steady-state fusion requires a predominantly self-driven plasma current and high β_N. Here, transport, stability and current profiles become mutually dependent – a self-consistent solution must be found and behavior at high β_N understood. DIII-D has used its flexible heating and current drive systems to make advances on three promising paths.

For a fusion power plant, scenarios with high β_N potential are key to optimizing bootstrap current and fusion performance. High q_{min} scenarios exploit broad current and pressure profiles (using DIII-D's off axis neutral beams and ECCD) to raise the with-wall ideal MHD β_N limit, though these sometimes encounter enhanced fast ion transport. Developing this regime to high β_P has enabled previous confinement limitations to be overcome through formation of an internal transport barrier, and/or higher pedestal, and reduction of peaking in fast ion profiles to improve AE stability (Fig. 20) [33]. This provides excellent thermal confinement (H_{98pby2}=1.5) and nearly classical fast ion confinement. These plasmas are sustained with 80% bootstrap current for two current redistribution timescales, providing a target regime for long pulse assessments in the superconducting EAST facility [34]. Further DIII-D work will focus on

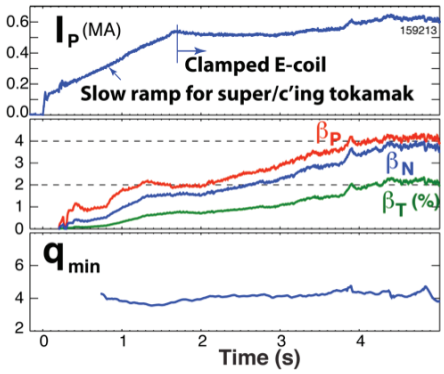

Fig. 20: Fully noninductive high β_P regime.

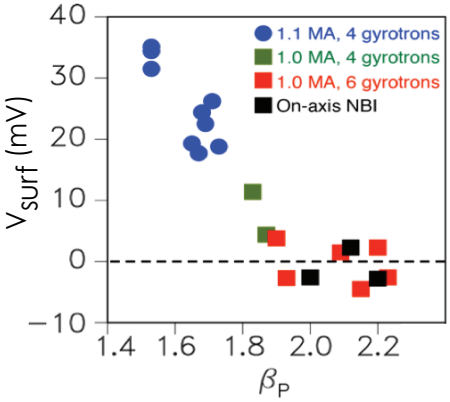

Fig. 21: 1 MA fully noninductive steady state hybrid β_P regime.

extending to higher β_T for a higher equivalent Q.

For a Fusion Nuclear Science or Component Test Facility (FNSF/CTF), a more centrally peaked current and higher performance hybrid scenario has been developed using Neutral Beam and ECH current drive to sustain 1 MA current fully non-inductively (Fig. 21) at β_N=4 and 40% Greenwald density [35]. 50% externally driven current combines with 50% bootstrap to sustain the discharge in stationary conditions for more than a current redistribution timescale. Confinement is excellent (H_{98}=1.7), optimizing towards higher density, with peak β_N values limited to 4.3 by energetic particle and tearing modes. The current profile is naturally regulated by benign core tearing modes to maintain q_{min}>1. This enables the regime to be readily sustained with efficient on-axis current drive, making it attractive for an FNSF or ITER. Encouragingly, RMP-ELM suppression has also been demonstrated in the ITER-shaped plasmas in this scenario [1].

An alternative path to steady states lies in plasmas with a more peaked current profile – the "high l_i" scenario [36]. This can raise the ideal MHD limit to β_N>5, while offering excellent confinement. Here, the current profile was optimized through pre-forming at low β and freezing it in with ECCD to avoid a β collapse with the first ELM that terminated previous attempts. In an ITER shape this led to Q_{eq}=5 performance (Fig. 22), providing an attractive candidate for ITER steady state using its day-one heating systems. In a double-null shape, β_N close to 5 was achieved (Fig. 17) with H_{98}=1.8 and 80% bootstrap current, leading to some current overdrive. Full stationarity is predicted with planned increases in ECH current drive power.

7. Developing a Boundary Solution for Fusion Energy

A boundary solution for future reactors represents one of the remaining grand challenges for fusion energy. This must go beyond present radiative techniques to establish an essentially detached, erosion free divertor. It requires optimization in divertor geometry and the plasma-materials interface (PMI). Thus, a new initiative has been launched to develop the basis for next step fusion development, to be tested in DIII-D.

Experiments have identified physics and shortfalls in the understanding of divertor detachment. Significant progress has been made in model validation, reproducing divertor parallel transport along field lines in well attached plasmas. New 2D mapped divertor Thomson scattering measurements show a sharp transition to detachment with increasing separatrix density (Fig. 23) [37,38], which is presently not easily reproduced in simulation. Comparison of detachment data with simulation also reveals a radiation shortfall (Fig. 24), with the UEDGE and SOLPS models only matching the experimental

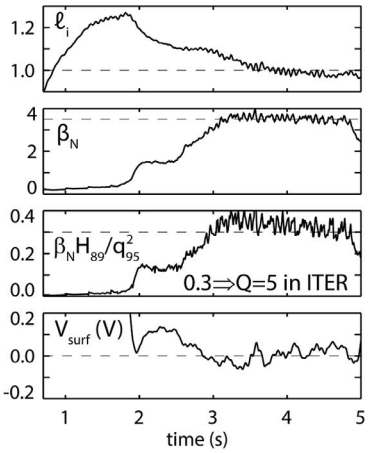

Fig. 22: ITER demonstration high l_i scenario.

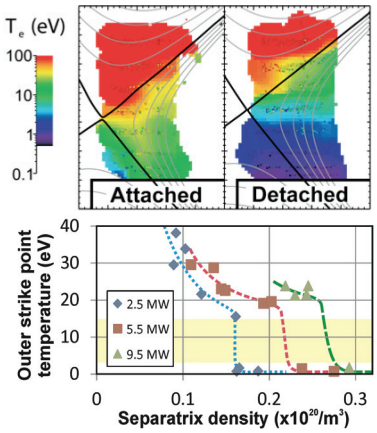

Fig. 23: Detachment onset thresholds from divertor TS.

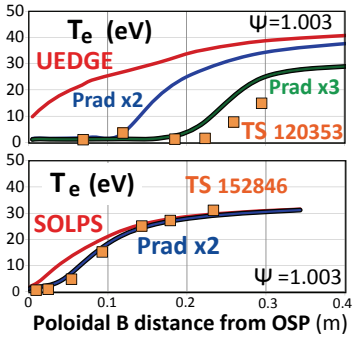

Fig. 24: Detachment shortfall in simulation codes (L mode).

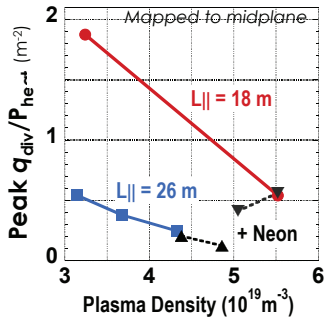

Fig. 25: Connection length effect on approach to detachment.

radiated power data once carbon levels are raised above experimental estimates, suggesting improved treatment of cold, molecular and atomic species is needed. H-mode comparisons yields a similar shortfall, though it is important to note further discrepancies at intermediate densities. Interestingly, helium plasmas detach at a higher temperature, 3 eV, indicating that molecular radiation plays an important role in D_2 plasmas. Plasma geometry is a key element in divertor optimization, with increased connection length found to detach plasmas more readily at lower core densities (Fig. 25) [39] where radiative power and cross field transport increasing in importance as the divertor leg is lengthened, reducing heat flux to the divertor. Similarly, a snowflake divertor leads to a decrease in peak scrape-off layer heat flux compared to standard divertor configurations [40]. Upstream scrape-off layer profiles exhibited a critical gradient behavior, consistent with ideal ballooning limits from low density up to divertor detachment. These elements are helping improve models for developing advanced divertor concepts.

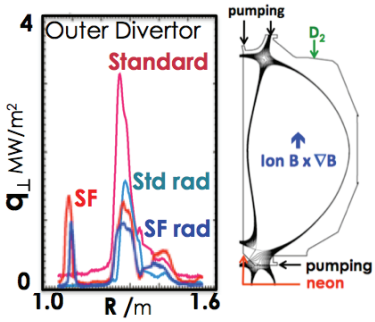

Fig. 26: Radiative standard and snowflake divertors with steady state plasmas.

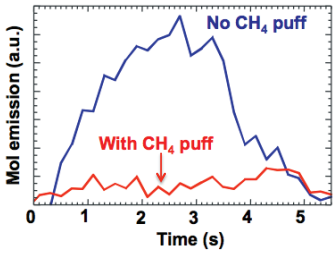

Fig. 27: Low Z coating prevents high Z erosion.

Techniques have been integrated into plasma operating scenarios yielding good performance and insights into optimization. It is found that impurity accumulation from a neon radiative divertor could be controlled by D_2 puffing to yield 80% radiation in ITER scenarios [31]. In steady-state DND plasmas, neon injection into the private flux region and away from the ion B×∇B direction reduces core impurity rises, to maintain H_{98}=1.3 performance while halving divertor heat flux (Fig. 26). Steady state has also been combined with the radiative snowflake divertor to yield modest further reductions in heat flux compared to standard radiative divertor, although the snowflake reduces impurity control.

DIII-D also provides an important qualifying stage for developing PFC solutions using the Divertor Material Evaluation System (DIMES) to expose and study material interactions with tokamak plasmas [41]. Experiments have confirmed that net erosion of tungsten divertor surfaces to be weak, with gross erosion largely compensated by redeposition. This work validated models that indicate low net erosion in the ITER divertor. For areas of particular concern outside the divertor, a new technique is demonstrated with renewable low Z coatings that are found effective in reducing erosion. CH_4 puffing near the sample leads to a carbon layer and factor of >10 reduction in molybdenum erosion (Fig. 27). This paves the way for other low Z elements (B, Si, Li) as potential protective layers against transients such as large ELMs or disruptions. Studies are now turning to validation of advanced materials for the reactor environment through testing of samples exposed in linear facilities such as PISCES.

8. Conclusions and Future Plans

DIII-D has made key advances in physics understanding required for ITER and fusion energy development. Promising ELM stable solutions have been extended in key parameters, and understood. Predictive models of pedestal behavior have been validated and new regimes discovered. Effective thermal and runaway mitigation techniques have been developed and characterized, qualifying new solutions for ITER. Studies are also identifying the new physics as we turn toward burning plasma conditions with torque free electron heating, while the dynamics of fast ions are becoming better understood with fully non-linear models, full 3D representations, and a newly identified critical gradient behavior. A 3D magnetic upgrade has

delivered critical understanding of plasma response, underpinning better error field, ELM and rotation control. The ITER baseline scenario has been extended to ITER-relevant torque, without a reduction in Q_{eq} associated with continuous ECCD mode control. However, should tearing modes occur, real time tracking techniques have been extended to routine operation even in the highest β_N scenarios. Three new steady state scenarios are developed to variously match ITER, FNSF and DEMO needs. Substantial steps in understanding detachment and its optimization through geometry and radiation have been made in the quest to define a better divertor concept. These developments provide key solutions for ITER and a foundation of understanding in order to project behavior and develop the means to safely achieve the required performance in future fusion reactors.

Turning to the future, studies in DIII-D will focus on three critical initiatives, where anticipation of behavior and development of new solutions is vital:

(i) **Prepare for Burning Plasmas** – to anticipate the changes in thermal, particle, momentum and fast ion transport that will happen with low torque electron heating dominant conditions by deploying toroidally steerable beams and ECH in order to understand the behavior and optimization of fusing plasmas

(ii) **Determine the Path to Steady State** – to develop a high β, self consistent, fully non-inductive, predominantly self-driven solution for fusion energy and an FNSF, with increased off-axis heating and current drive by increasing both the neutral beam total and off-axis power, ECCD and developing helicon ultra fast wave current drive [42].

(iii) **Develop a Boundary–PMI Solution** – to achieve an erosion free detached divertor solution compatible with a high performance self-driven core and PFC materials, by implementing an advanced divertor, reactor relevant hot walls and advanced 3D field coil set.

These improvements will enable DIII-D to provide vital input to the ITER mission, in developing both the techniques to meet its performance goals and the models to project and interpret behavior. However, they are even more critical for a future steady state reactor, such as DEMO or FNSF, which cannot be designed until the requirements for a high performance core and a viable boundary solution with adequate exhaust mitigation are developed.

This work was supported in part by the US Department of Energy under DE-FC02-04ER54698, DE-FG02-89ER54297, and DE-AC02-09CH11466.

References

[1] Nazikian, R. et al., this conference EX/1-1.
[2] Nazikian, R. et al., submitted to Phys. Rev. Lett.
[3] Paz-Soldan, C. et al., submitted to Phys. Rev. Lett.
[4] Evans, T.E. et al., this conference EX/1-3.
[5] Orlov, D.M. et al., this conference EX/P2-21.
[6] Snyder, P.B. et al., Nucl. Fusion **51** (2011) 103016.
[7] Solomon,W.M. et al., this conference PPC/P2-37.
[8] Liu, F. et al., Proc. 41st EPS (2014) O5.135.
[9] Snyder, P.B. et al., this conference TH/2-2.
[10] Jackson, G.L. et al., this conf. postdeadline.
[11] Diallo, A. et al., this conference EX/3-2
[12] Battaglia, D.J. et al., this conference EX/P2-24.
[13] Yan, Z. et al., Phys. Rev. Lett. **112** (2014) 125002
[14] Schmitz, L., et al., this conference EX/11-4.
[15] Staebler, G.M. et al., this conference TH/P5-12.
[16] Paz-Soldan, C. et al., Phys Plasmas **21** (2014) 022514.
[17] Eideitis, N.W. et al., this conf., postdeadline
[18] Eidietis, N.W. et al. this conference EX/P2-22.
[19] Izzo, V.A. et al., this conference TH/4-1.
[20] McKee, G.R. et al., this conference EX/2-2.
[21] Ernst, D.R. et al., this conference EX/2-3.
[22] Mordjick, S. et al., this conference EX/P2-30.
[23] Angioni, C. et al., Phys. Plasmas **12** (2005) 040701
[24] Smith, S. et al., this conference EX/P2-29.
[25] Heidbrink, W. et al., this conference EX/10-1.
[26] Collins, C., submission to Phys. Rev. Lett.
[27] Todo, Y. et al., this conference TH/7-1.
[28] Van Zeeland, M.A. et al., this conf. EX/10-2.
[29] Paz Soldan, C. et al., this conf. EX/P2-28
[30] Lanctot, M.J. et al., this conf., postdeadline.
[31] Luce, T.C. et al., this conference PPC/P2-34.
[32] Hawryluk, R.J. et al., this conference PPC/P2-33.
[33] Garofalo, A.M. et al, this conference PPC/P2-31.
[34] Gong, X. et al., this conference EX/P2-39.
[35] Petty, C.C., et al. this conference PPC/P2-36.
[36] Ferron, J.R. et al., this conference PPC/P2-35.
[37] McLean, A.G. et al. this conference EX/P2-18.
[38] Kolemen, E. et al., this conference PPC/1-1.
[39] Petrie, T.W. et al., this conference EX/P2-26.
[40] Soukhanovskii, V.A. et al., this conf. EX/7-4.
[41] Rudakov, D.L. et al., this conference EX/P2-27
[42] Pinsker, R.I. et al., this conference TH/P2-38.

DIII-D Team

L. Abadie[1], G. Abla[2], J.W. Ahn[3], E. Allen[2], S.L. Allen[4], G. Ambrosino[5], J.P. Anderson[2], R.G. Andre[6], C. Angioni[7], J.F. Artaud[8], M.E. Austin[9], J.G. Bak[10], J.P. Bakalarski[2], L. Bardoczi[11], J.E. Barton[12], M. Baruzzo[13], E.M. Bass[14], D. Batchelor[3], D.J. Battaglia[6], D.A. Baver[15], L.A. Baylor[3], G. Bell[3], E.A. Belli[2], L.A. Berry[16], N. Bertelli[6], J.M. Bialek[17], B.D. Blackwell[18], J.A. Boedo[14], R.L. Boivin[2], T. Bolzonella[13], M.D. Boyer[12], D.P. Boyle[6], R.V. Bravenec[19], B.D. Bray[2], A.R. Briesemeister[3], N.H. Brooks[2], J.N. Brooks[20], W.D. Brown[6], D.A. Buchenauer[21], R.V. Budny[6], K.H. Burrell[2], R.J. Buttery[2], J.D. Callen[22], R.W. Callis[2], G.L. Campbell[2], J. Candy[2], J.M. Canik[3], T.N. Carlstrom[2], T.A. Carter[11], W.P. Cary[2], T.A. Casper[1], M. Cengher[2], F.R. Chamberlain[2], V.S. Chan[2], C.S. Chang[6], B. Chanthavong[2], J.A. Chavez[2], S. Che[23], B. Chen[2], X. Chen[2], Y. Chen[24], R. Chipman[25], H. Choi[2], M. Choi[2], C.P. Chrobak[2], C. Chrystal[14], M.S. Chu[2], I.G.J. Classen[26], C.M. Collins[27], S. Combs[3], N. Commaux[3], R. Coon[2], K. Crabtree[25], N.A. Crocker[11], B. Crowley[2], I. Cziegler[14], E.M. Davis[28], B.M. Davis[6], G. de Tommasi[5], J.C. Deboo[2], J.S. deGrassie[2], T.M. Deterly[2], A. Diallo[6], P.H. Diamond[14], S.J. Diem[3], S. Ding[29], P. Diwakar[20], A.M. Dmits[4], J.L. Doane[2], R. Doerner[14], C.W. Domier[23], D.C. Donovan[21], E.J. Doyle[11], N.W. Eidietis[2], J.D. Elder[30], D.P. Eldon[14], R.E. Ellis[4], R.A. Ellis[6], D.R. Ernst[28], T.E. Evans[2], M. Fahey[3], G. Falchetto[8], D. Fehling[3], M.E. Fenstermacher[4], N.M. Ferraro[2], J.R. Ferron[2], D.F. Finkenthal[31], R.K. Fisher[2], S.M. Flanagan[2], R.J. Fonck[22], C Foust[3], D.P. Fulton[27], M. Garcia-Munoz[7], A.M. Garofalo[2], S.P. Gerhardt[6], P. Gohil[2], X. Gong[29], N.N. Gorelenkov[6], Y.A. Gorelov[2], R. Granetz[28], T.K. Gray[3], K.L. Greene[2], C.M. Greenfield[2], N.L. Greenough[6], M. Greenwald[28], Y. Gribov[1], B.A. Grierson[6], L. Grisham[6], R.J. Groebner[2], M. Groth[32], H.J. Grunloh[2], H.Y. Guo[2], P. Gupta[2], W. Gutetenfelder[6], T.J. Guzman[2], M.J. Hansink[2], J.M. Hanson[17], G.R. Hanson[3], J.H. Harris[3], S.R. Haskey[18], A. Hassanein[20], R.J. Hawryluk[6], G. Heber[33], W.W. Heidbrink[27], D.N. Hill[4], J.C. Hillesheim[11], D.L. Hillis[3], S.P. Hirshman[3], C.T. Holcomb[4], C. Holland[14], E.M. Hollmann[14], I. Holod[27], K.L. Holtrop[2], A.R. Horton[3], J.C. Hosea[6], J. Hou[34], J. Howard[18], X. Hu[23], A.E. Hubbard[28], B. Hudson[3], J.W. Hughes[28], G. Huijsmans[1], D.A. Humphreys[2], P. Huynh[2], A.W. Hyatt[2], K. Ida[35], Y. In[36], S. Inagaki[37], J. Irby[28], R.C. Isler[3], K.N. Ivanov[34], O. Izacard[14], V.A. Izzo[14], G.L. Jackson[2], E.F. Jaeger[16], A.N. James[4], T.C. Jernigan[3], R.D. Johnson[2], I. Joseph[4], D.H. Kaplan[2], M.C. Kaufman[3], K.M. Keith[2], A.G. Kellman[2], D.H. Kellman[2], C.E. Kessel[6], J.D. King[2], J.E. Kinsey[38], W-H. Ko[10], T. Kobayashi[35], M. Kocan[1], E.R. Koch[2], E. Kolemen[6], T. Koskela[32], G.J. Kramer[6], A. Kritz[12], S. Ku[6], J.A. Kulchar[2], C.C. Kung[6], T. Kurki-Suonio[32], R.J. La Haye[2], B. LaBombard[28], T. Lambot[18], M.J. Lanctot[2], M. Landreman[28], L.L. Lao[2], C.J. Lasnier[4], C. Lau[3], E.A. Lazarus[3], S.A. Lazerson[6], R.L. Lee[2], X. Lee[2], A.W. Leonard[2], G. Li[29], A. Lietz[24], Z. Lin[27], J.B. Lister[39], A. Litnovsky[40], F. Liu[8], Y.Q. Liu[41], C. Liu[2], F. Liu[1], A. Loarte[1], N.C. Logan[6], J. Lohr[2], J.D. Lore[3], T.C. Luce[2], N.C. Luhmann, Jr.[23], C. Luna[42], G.N. Luo[29], R. Maggiora[43], J.E. Maggs[11], M.A. Mahdavi[44], R. Maingi[6], M.A. Makowski[4], D.K. Mansfield[6], P. Mantica[45], A. Marinoni[28], E.S. Marmar[28], L. Marrelli[13], P. Martin[13], J. Martin-Solis[46], M. Mattei[47], P.S. Mauzey[2], W.L. McDaniel[2], G.R. McKee[22], A.G. McLean[4], S. Meitner[3], J.E. Menard[6], O. Meneghini[48], W.H. Meyer[4], D.R. Mikkelsen[6], D. Milanesio[43], D.C. Miller[2], C.P. Moeller[2], G.J. Morales[11], S. Mordijck[49], D. Moreau[8], K. Morris[4], R.A. Moyer[14], D. Mueller[6], J.M. Munoz-Burgos[48], T. Munsat[24], D.D. Murakami[50], M. Murakami[3], C.J. Murphy[2], C.J. Murphy[6], C.M. Muscatello[23], J.A. Myra[15], L. Myrabo[51], A. Nagy[6], G.A. Navratil[17], R. Nazikian[6], G. Neu[7], X. Nguyen[11], J.H. Nichols[6], D. Nishijima[14], S. Noraky[2], R. Nygren[21], M. O'Mullane[4], R.C. O'Neill[2], S. Ohdachi[35], M. Okabayashi[6], K.E.J. Olofsson[17], D.M. Orlov[14], T.H. Osborne[2], L.W. Owen[3], R. Paccagnella[13], D.C. Pace[2], A.Y. Pankin[52], J.M. Park[3], J.-K. Park[6], C.T. Parker[2], S.E. Parker[24], K.L. Parkin[18], P.B. Parks[2], C.J. Pawley[2], C. Paz-Soldan[2], W.A. Peebles[11], B.G. Penaflor[2], R.J. Perkins[6], T.W. Petrie[2], C.C. Petty[2], D.A. Piglowski[2], R.I. Pinsker[2], P. Piovesan[13], R. Pipes[24], C. Piron[13], L. Piron[13], R.A. Pitts[1], M. Podesta[6], F.M. Poli[6], P.A. Politzer[2], D.M. Ponce[2], M. Porkolab[28], G.D. Porter[4], R. Prater[2], J. Qian[29], T. Rafiq[12], R. Raman[53], J. Rauch[2], P.T. Raum[54], G. Raupp[7], A. Reiman[6], H. Reimerdes[39], Q. Ren[29], X. Ren[23], T.L. Rhodes[11], J. Rice[28], P. Riemenschneider[23], D. Robinson[33], A. Romosan[55], A.L. Roquemore[6], J.C. Rost[28], D.L. Rudakov[14], P.M. Ryan[3], D.D. Ryutov[4], A. Salmi[56], B.S. Sammuli[2], M.J. Schaffer[2], D.P. Schissel[2], R.W. Schleicher[2], L. Schmitz[11], O. Schmitz[22], K.R. Schultz[2], E. Schuster[12], J.T. Scoville[2], L.G. Seppala[4], M.W. Shafer[3], W. Shi[12], L. Shi[6], K. Shinohara[57], S. Shiraiwa[28], D. Shiraki[3], K.C. Shoolbred[2], A. Shoshani[55], P.E. Sieck[2], T. Sizyuk[20], S.P. Smith[2], J.A. Snipes[1], P.B. Snyder[2], W.M. Solomon[6], A.C. Sontag[3], V.A. Soukhanovskii[4], K.H. Spatschek[58], A. Spear[23], D.A. Spong[3], H.E. St John[2], W.M. Stacey[59], G.M. Staebler[2], L. Stagner[27], P.C. Stangeby[30], R. Stemprok[2], J. Stillerman[28], T.J. Stoltzfus-Dueck[6], H. Stoschus[48], E.J. Strait[2], M. Sugihara[60], L.E. Sugiyama[28], W. Suttrop[7], T. Suzuki[57], Y. Suzuki[35], R.M. Sweeney[17], H. Takahashi[6], T. Tala[61], K. Tanaka[35], R. Tao[2], D.A. Taussig[2], P.L. Taylor[2], T.S. Taylor[2], G. Taylor[6], D. Terranova[13], J.L. Terry[28], D.M. Thomas[2], B.J. Tobias[6], J.F. Tooker[2], A.C. Torrezan[2], W. Treutterer[7], J. Tripathi[20], D. Truong[22], C. Tsui[30], F. Turco[17], A.D. Turnbull[2], G.R. Tynan[14], M.V. Umansky[4], E.A. Unterberg[3], D. Urone[4], E. Valeo[6], M.A. Van Zeeland[2], V.L. Vdovin[62], R. Vieira[28], S. Visser[2], F. Volpe[17], M.R. Wade[2], J. Walk[28], M.L. Walker[2], D. Wall[2], G. Wallace[28], A. Wallander[1], R.E. Waltz[2], W.R. Wampler[21], B. Wan[29], W. Wan[24], W.X. Wang[6], Z.R. Wang[6], X. Wang[49], G. Wang[11], C.W. Wannberg[11], M.G. Watkins[2], J.G. Watkins[21], W.P. Wehner[12], A.S. Welander[2], J.C. Wesley[2], A.E. White[28], D.G. Whyte[28], H.R. Wilson[63], A. Wingen[3], A. Winter[1], S.M. Wolfe[28], C.P.C. Wong[2], S.K. Wong[2], G.M. Wright[28], J. Wright[28], M. Wright[64], W. Wu[2], W.W. Xiao[6], G. Xu[29], X.Q. Xu[4], Z. Yan[22], L. Yu[23], J.H. Yu[14], X. Yuan[6], P. Zanca[13], S. Zemedkun[24], L. Zeng[11], J. Zhang[11], Y. Zhao[22], G. Zhong[65], Y.B. Zhu[27], S.J. Zweben[6].

DIII-D Collaborators

[1] ITER Organization, St. Paul Lez Durance, FR
[2] General Atomics
[3] Oak Ridge National Laboratory
[4] Lawrence Livermore National Laboratory
[5] CREATE/Università di Napoli Federcico II, Napoli, Italy
[6] Princeton Plasma Physics Laboratory
[7] Max-Planck-Institut fu¨r Plasmaphysik, Garching
[8] CEA, IRFM, Saint-Paul-lez-Durance, France
[9] University of Texas at Austin
[10] National Fusion Research Center, Korea
[11] University of California Los Angeles
[12] Lehigh University
[13] Consorzio RFX, Ricerca Formazione Innovazione, Padova, Italy
[14] University of California San Diego
[15] Lodestar Research Corporation, Boulder, CO
[16] XCEL Engineering, Oak Ridge, TN
[17] Columbia University
[18] Australian National University, Canberra
[19] Fourth State Research, Austin, TX
[20] Purdue University
[21] Sandia National Laboratories
[22] University of Wisconsin-Madison
[23] University of California at Davis
[24] University of Colorado at Boulder
[24] University of Hawaii, Hilo, HI
[24] University of Illinois
[25] University of Arizona, Tucson
[26] FOM-Institute DIFFER
[27] University of California Irvine
[28] Massachusetts Institute of Technology
[29] Chinese Academy of Sciences, Institute of Plasma Physics, Hefei, PRC
[30] University of Toronto Institute for Aerospace Studies
[31] Palomar College, San Marcos
[32] Aalto University, Association EURATOM-Tekes, Espoo, Finland
[34] The Pennsylvania State University
[35] National Institute for Fusion Sciences, Toki Gifu, Japan
[36] FAR-TECH, Inc.
[37] RIAM, Kyushu University, Japan
[38] CompX
[39] Ecole Poytechnique Federale Lausanne (EPFL), CRPP, Euratom Association, Lausanne, Switzerland
[40] Forschungszentrum, Julich, GmbH
[41] Culham Centre for Fusion Energy (CCFE)
[42] Arizona State University
[43] Politecnico di Torino, Dipartimento di Elettronica
[44] ALITRON, Inc
[45] Istituto di Fisica del Plasma, Associazione Euratom-ENEA-CNR, Milano, Italy
[46] Universidad Carlos III, Leganes, Spain.
[47] Seconda Università di Napoli, Napoli, Italy
[48] Oak Ridge Institute for Science and Education
[49] The College of William and Mary
[50] NASA Ames Research Center, CA
[51] Lightcraft Technologies, Inc., Vermot
[52] Tech-X, Boulder, CO
[53] University of Washington, Seattle
[54] Virginia Tech, Blacksburg
[55] Lawrence Berkeley National Laboratory
[56] Association EURATOM-Tekes, Aalto University, Department of Applied Physics, Finland
[57] Japan Atomic Energy Agency
[58] Institut für Theoretische Physik, Heinrich-Heine-Universit at Düsseldorf
[59] Georgia Institute of Technology
[60] ITER Organization, St. Paul Lez Durance, FR (Retired)
[61] Association Euratom-Tekes, VTT, PO Box 1000, FIN-02044 VTT, Finland
[62] Kurchatov Institute, Russia
[63] York Plasma Institute, University of York, UK
[64] Ultramet, Pacoima, CA
[65] Southwestern Institute of Physics, Chengdu, PRC